

# Modal analysis using photonic lanterns coupled to arrays of waveguides

MOMEN DIAB<sup>1,\*</sup> AND STEFANO MINARDI<sup>2</sup>

<sup>1</sup>innoFSPEC - Leibniz Institute for Astrophysics Potsdam, An der Sternwarte 16, 14482 Potsdam, Germany.

<sup>2</sup>LASOS GmbH, Franz-Löwen Str. 2, 07745 Jena, Germany.

\*Corresponding author: mdiab@aip.de

Compiled March 13, 2019

We present a new concept of an integrated optics component capable of measuring the complex amplitudes of the modes at the tip of a multimode waveguide. The device uses a photonic lantern to split the optical power carried by an  $N$ -modes waveguide among a collection of single-mode waveguides that excite a periodic array of at least  $N^2$  single-mode evanescently-coupled waveguides. The power detected at each output of the array is a linear combination of the products of the modal amplitudes—a relation that can, under suitable conditions, be inverted allowing the derivation of the amplitudes and relative phases of the modal mixture at the input. The expected performance of the device is discussed and its application to the real-time measurement of modal instability in high power fiber lasers is proposed.

© 2019 Optical Society of America

**OCIS codes:** (120.5050) Phase measurement, (120.4640) Optical instruments, (030.4070) Modes, (080.1238) Array waveguide devices, (060.2420) Fibers.

<http://dx.doi.org/10.1364/ao.XX.XXXXXX>

The decomposition of the optical field carried by a multimode fiber into its supported modes is a requirement for several applications in the photonic industry ranging from spatial division multiplexing communication protocols [1] to management of modal instability in high power fiber lasers [2]. However, while modal decomposition of an optical field is a straightforward numerical task, it is usually a rather complex one from the experimental viewpoint. Free space modal characterization techniques often use phase holograms as multiplexed mode matched filters [3] to retrieve amplitude and phase from optical cross-correlations of the mode functions with the fiber field [4]. Direct field measurement by means of a wavefront sensor [5] or by means of a spatial-spectral scan of the mode profile [6] are other free space methods used to estimate the modal coefficients in an excited fiber. A common

feature of free space methods is the requirement of extended setups and slow data processing, making them unsuitable for high speed applications. Integrated optics mode-division multiplexer/demultiplexer can offer devices with smaller footprints and a fast measurement of the modulus of the modal (complex) amplitude. In this respect, asymmetric couplers in 2 [7] and 3 dimensions [8, 9] and asymmetric photonic lanterns [10] have been used to multiplex/demultiplex up to 3 modes in rectangular multimode waveguides. While the speed of the modal decomposition in demultiplexers is limited by the speed of the light detector at the output, an integrated device measuring the relative phase between the excited modes has not been reported so far. The measurement of the modal phase is an essential requirement to determine the exact optical pattern at the output plane of the multimode fiber, information that could find application in the active control of modal instability in high power fiber lasers [11].

In this letter we present the concept of a new integrated optics device designed to accomplish a complete measurement of the complex modal amplitudes at the input of a multimode waveguide [12]. The proposed device combines a photonic lantern [13] with a discrete beam combiner [14], as sketched in Fig. 1. After describing the operating principle, we present the results of a numerical optimization of the device and discuss estimates of the precision of the modal complex amplitude retrieval relative to detection noise.

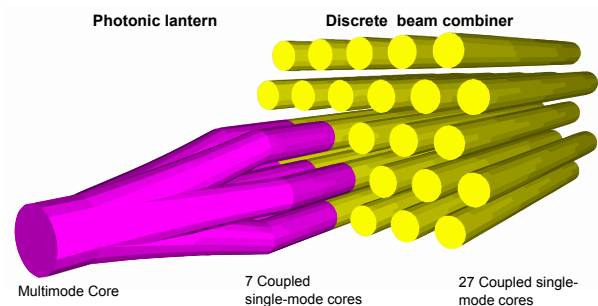


**Fig. 1.** Layout of a photonic mode analyzer designed to retrieve the complex amplitudes of the modes excited at its multimode input. The scale in the propagation direction is reduced by 200x relative to the transverse coordinates and the cladding of the waveguides is hidden for clarity.

As known, the photonic lantern is a tapered waveguide that transforms adiabatically the modes supported by its multimode end into the supermodes of an array of single-mode waveguides. The output of the lantern can be used to excite an array of coupled single-mode waveguides, designed to act as an interferometric beam combiner, i.e., the discrete beam combiner. We show here below that by choosing appropriately the interface between the photonic lantern and the discrete beam combiner, it is possible to relate linearly the power carried by each output of the beam combiner with the square moduli and mutual products of the input modal amplitudes.

We begin by describing our system in terms of a linear operator  $\hat{\psi}$  from the  $N$ -dimensional functional space spanned by the transverse modes  $U_i(x, y)$  of the multimode end of the lantern to an  $M$ -dimensional functional space describing the excitations of the  $M$  waveguides of the discrete beam combiner. In the frame of the coupled-mode approximation, the fields supported by the array of evanescently-coupled waveguides are written in terms of the mode profile  $u_0(x, y)$  of the isolated single-mode waveguide, each centered at the coordinates  $(x_n, y_n)$  of the  $n$ th waveguide axis. With this approximation, we can choose as a base of the  $M$ -dimensional space, fields composed of single waveguide excitations at the output of the array  $u_n(x, y) = u_0(x - x_n, y - y_n)$ . We can thus rewrite the operator  $\hat{\psi}$  as an  $M \times N$  complex matrix  $\psi_{n,i} = \langle u_n | \hat{\psi} U_i \rangle$ , where the norm  $\langle \cdot | \cdot \rangle$  is the usual overlap integral. Notice that  $\psi_{n,i}$  represents the complex amplitude of the mode of the  $n$ th waveguide at the output of the array due to an excitation of the photonic lantern input with mode  $U_i$ . If the transition from multimode end to array output is lossless and the chosen bases are normalized we clearly have that  $\sum_{n=1}^M |\psi_{n,i}|^2 = 1$  for every  $i = 1, \dots, N$ . A generic superposition of the input modes  $U_i$  with weights  $c_i \in \mathbb{C}$  will therefore map into the output amplitude

$$\phi_n = \sum_{i=1}^N c_i \psi_{n,i}, \quad n = 1, \dots, M. \quad (1)$$

We now consider that powers rather than fields are measured at the output waveguides, i.e., with a detector array aligned with the waveguides. Because we assume that the chosen base is orthonormal, the signal  $I_n$  of the detector is

$$I_n = \left| \sum_{i=1}^N c_i \psi_{n,i} \right|^2, \quad (2)$$

which can be written in the following expanded form:

$$I_n = \sum_{i=1}^N |c_i|^2 |\psi_{n,i}|^2 + 2 \sum_{i=1}^{N-1} \sum_{j=1}^N [\Re(c_i c_j^*) \Re(\psi_{n,i} \psi_{n,j}^*) - \Im(c_i c_j^*) \Im(\psi_{n,i} \psi_{n,j}^*)], \quad (3)$$

where the operators  $\Re(z)$  and  $\Im(z)$  denote the real and imaginary parts of  $z$ , respectively. For all output waveguides, the equations in Eq. (3) can be arranged in a matrix form:

$$\vec{I} = \mathbf{V} \cdot \vec{J}. \quad (4)$$

By choosing the  $N^2$ -dimensional vector  $\vec{J}$  as

$$\vec{J} = [|c_1|^2, \dots, |c_N|^2, \Re(c_1 c_2^*), \dots, \Re(c_{N-1} c_N^*), \Im(c_1 c_2^*), \dots, \Im(c_{N-1} c_N^*)]^T, \quad (5)$$

the matrix  $\mathbf{V}$  can be divided into three sub-matrices  $\mathbf{V} = [\mathbf{A} : \mathbf{B} : \mathbf{C}]$  where  $\mathbf{A}$  is an  $M \times N$  matrix that contains the squared moduli of  $\psi_{n,i}$  while  $\mathbf{B}$  and  $\mathbf{C}$  are matrices of size  $M \times N(N-1)/2$  that contain the real and imaginary parts of all possible pair products  $\psi_{n,i} \psi_{n,j}^*$ , respectively. The entries of  $\mathbf{A} = [\alpha_{i,j}]$ ,  $\mathbf{B} = [\beta_{i,j'}]$  and  $\mathbf{C} = [\gamma_{i,j'}]$  are given explicitly by

$$\begin{aligned} \alpha_{i,j} &= |\psi_{i,j}|^2, \\ \beta_{i,j'} &= 2\Re(\psi_{i,p(j')} \psi_{i,q(j')}^*), \\ \gamma_{i,j'} &= -2\Im(\psi_{i,p(j')} \psi_{i,q(j')}^*), \end{aligned} \quad \begin{aligned} i &= 1, \dots, M, \\ j &= 1, \dots, N, \\ j' &= 1, \dots, N(N-1)/2, \end{aligned} \quad (6)$$

where  $p(j')$  and  $q(j')$  are given by

$$\begin{aligned} p(j') &= m, \quad \text{for } m \in \mathbb{N} \text{ that satisfies} \\ (m-1) \left( N - \frac{m}{2} \right) &< j' \leq m \left( N - \frac{m+1}{2} \right), \\ q(j') &= p(j') + j' + [p(j') - 1] \left[ \frac{1}{2} p(j') - N \right]. \end{aligned} \quad (7)$$

Now  $\mathbf{V}$  in Eq. (4) has a generalized inverse provided that its number of rows  $M \geq N^2$ , i.e., the discrete beam combiner section of the device must at least have a number of coupled waveguides equal to the square of the number of modes to be analyzed.

While the numerical determination of the matrix  $\mathbf{V}$  is straightforward, in a real experiment a calibration procedure is required. This can be accomplished with a method similar to the one used for the calibration of integrated optics interferometers for astronomical use (see for instance [15]). In the present case, a spatial light modulator is required to excite selectively the modes of the multimode end of the device and perform the calibration. In particular, the columns of the sub-matrix  $\mathbf{A}$  are obtained from the power delivered by each output waveguide resulting from the excitation of individual modes of the photonic lantern. The sub-matrices  $\mathbf{B}$  and  $\mathbf{C}$  are obtained by exciting the device with a superposition of modes with a linearly increasing phase delay between them.

The column vector  $\vec{J}$  [Eq. (5)] contains the square moduli of the coefficients  $c_i$  and the real and imaginary parts of all possible pair products of the modal amplitudes. Since only the relative phase between the modes matter to retrieve the input pattern of light, only the real and imaginary parts of the products of the amplitudes of a reference mode (e.g. the fundamental one) by the conjugate of the amplitudes of the other modes are indeed necessary to solve the modal decomposition problem. Solving for  $\vec{J}$  is equivalent to solving an overdetermined system of equations, which is possible by left multiplying the vector  $\vec{I}$  by the Moore-Penrose pseudoinverse of  $\mathbf{V}$ :  $\mathbf{V}^+ = (\mathbf{V}^T \mathbf{V})^{-1} \mathbf{V}^T$  [16]. An important feature of this solution algorithm is to gauge the sensitivity of the solution to the inevitable measurement noise of the elements of  $\vec{I}$ . This is possible by estimating the condition number of  $\mathbf{V}$ , which is defined as the ratio of the maximum to the minimum singular values of the matrix [16].

The condition number (which we denote with the symbol  $\kappa$ ) can be interpreted as the ratio of the maximal to minimal stretching ratios of the matrix  $\mathbf{V}$  along specific directions in the space of the  $\vec{J}$  vector. Thus, an ill-conditioned matrix (large  $\kappa$ )

would stretch the vectors much more in one direction than another meaning that small perturbations of the vector  $\vec{f}$  chosen along certain directions would be amplified greatly by the mapping operation. Therefore, a small  $\kappa$  is required to ensure the numerical stability of the transformation  $V$  and its pseudoinverse.

As it has been already shown in the past [17, 18], the conditioning of the transfer matrix  $V$  of a discrete beam combiner significantly depends on the geometric parameters of the waveguide array and its excitation configuration. To optimize the modal analyzer, we considered not only the geometry of the array of waveguides, but we also carried out tests to find a convenient injection geometry from the photonic lantern to the discrete beam combiner. A thorough verification of all injection configurations would become very rapidly an intractable problem due to their factorial scaling with the number of waveguides in the photonic lattice. We therefore used a heuristic method to guide our optimization process, which was based on the requirement of a field transfer function  $\psi_{i,j}$  with aperiodic phases evenly distributed on the  $0 - 2\pi$  interval [18]. The optimization was carried out by means of an RSoft CAD [19] model of the mode analyzer. The  $V$  matrices of the studied designs were constructed according to Eq. (6) from the peak amplitudes of the fields at the waveguides centers  $\psi_{i,j}$  calculated by the beam propagation solver BeamPROP [19]. The multimode end of the device has an  $8 \mu\text{m}$  core diameter and a numerical aperture of 0.17 and hence supports 3 LP modes (the fundamental  $\text{LP}_{01}$  and the doubly-degenerate  $\text{LP}_{11}$ ) at  $\lambda = 1.5 \mu\text{m}$  (see Fig. 1). The single-mode fibers emerging from the multimode core and the array's waveguides have a  $5 \mu\text{m}$  core diameter each with a similar numerical aperture. The lattice constant of the hexagonal array is  $7.5 \mu\text{m}$  which gives a coupling length of  $L_C = 1 \text{ mm}$ . The lantern's taper angle is taken shallow enough for it to be adiabatic.

Fig. 2 shows the dependence of  $\kappa$  on the array's length for some of the configurations we studied while attempting to optimize the device. This optimization strategy was supported by the observation that an input configuration where the output waveguides of the photonic lantern are symmetrically distributed across the array give rise to highly ill-conditioned  $V$

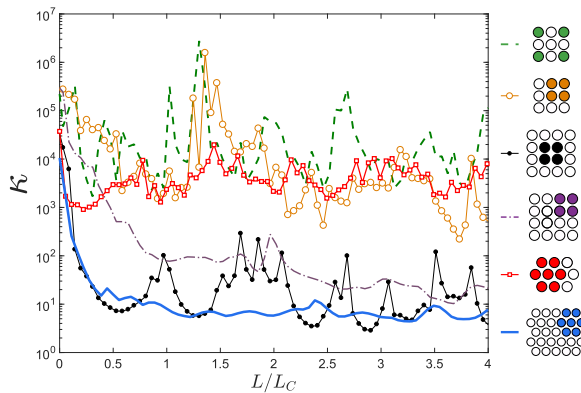


**Fig. 2.** (Color online) Variations of the condition number  $\kappa$  of  $V$  along the array in units of coupling lengths for different geometries. A hexagonal oversized array with an off-center  $1 \times 7$  lantern (— curve) provides the best performance as it has a low condition number that is fairly insensitive to length.

matrices (one example of this case is the configuration shown by --- in Fig. 2). For those configurations the modes of the photonic lantern excite with high efficiency the analogous real-valued supermodes of the photonic lattice, which allow only two possible phases separated by  $\pi$ . On the contrary, by restricting the injection sites to contiguous sites of the photonic lattice (see —○ in Fig. 2), the field propagating in the array is in general a complex-valued superposition of different supermodes, allowing the transfer function  $\psi_{i,j}$  to take arbitrary phase values. An off-center excitation of the array provided a smoother dependence of  $\kappa$  on the device's length (cf. --- and —○ in Fig. 2) as more phase diversity is introduced thanks to the broken symmetry of the system in agreement with previous results [18]. Additionally, the array needed to be compatible with the symmetry of the modes of the photonic lantern to avoid modal losses [20]. For this reason, we chose a  $1 \times 7$  photonic lantern supporting  $N = 3$  linearly polarized (LP) modes coupled to 7 neighboring sites of a hexagonal photonic lattice featuring more than 9 waveguides (see —□ in Fig. 2). We thus significantly restricted the number of configurations to be tested with a beam propagation method to a bare minimum. We confirmed that, even though the minimal number of waveguides required in the photonic lattice is  $M = N^2$  (in this case, 9 for the 3 modes), an oversized device with more waveguides leads to better conditioned matrices  $V$  (cf. —□ and — in Fig. 2). The phases at output waveguides corresponding to each of the supported modes for two of the configurations we studied are counted in the histograms in Fig. 3. The oversized hexagonal configuration (shown by — in Fig. 2 and by ■ in Fig. 3) which possesses all the attributes we deemed beneficial to lowering  $\kappa$  has its phases more evenly distributed in the interval  $[-\pi, \pi]$  than the phases of the square configuration (shown by --- in Fig. 2 and by ■ in Fig. 3), which lacks those attributes.

Fig. 1 illustrates the layout of a device with an optimized configuration. The device has been designed for an input lantern supporting 3 modes and has a minimal condition number of  $\kappa = 4.4$  (at array length  $L = 3.3 \text{ mm}$ ) as a result of the oversized array (27 waveguides). Interestingly, the condition number varies smoothly along the length of the device (Fig. 2, — curve), so that the performance of a real device is relatively tolerant to uncertainties in the coupling coefficient of the waveguide array.

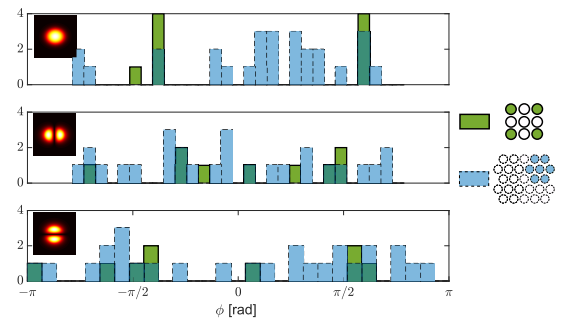


**Fig. 3.** (Color online) Histogram of the phase of the field transfer matrix  $\psi_{n,i}$  for  $i = 1, 2$  and  $3$  (excitation of the device with the 3 modes supported by the lantern and shown in the insets) in a 9 waveguides square array (■ fill,  $\kappa = 2 \times 10^6$ ) and a 27 waveguides hexagonal array with an off-center lantern (■ fill,  $\kappa = 4.4$ ). Greater phase diversity of the field transfer matrix yields  $V$  matrices with lower condition numbers.

The performance of the same device was evaluated numerically by calculating the impact of an additive random noise in the intensity measurement (e.g. dark current of a single pixel detector) on the retrieval of the complex amplitudes of the input modes. The algorithm computes the intensity signal at the output of the mode analyzer  $\tilde{I}$  from an array of different input vectors  $\tilde{J}$ , each one with unitary modal amplitude and a phase covering all possible combinations of relative phases between modes 1-2 and 1-3 sampled on the  $[0, 2\pi]$  interval. We added to each element of the calculated  $\tilde{I}$  vectors a random number with zero mean and Gaussian distribution of amplitude  $\epsilon$ . The noisy vector was transformed back to the modal amplitude vector  $\tilde{J}_\epsilon$  by means of the pseudoinverse of  $V$  and its average distance  $\chi$  from the input vector  $\tilde{J}$  was calculated:

$$\chi = \sqrt{\frac{\sum_{i=1}^{N^2} [J_\epsilon(i) - J(i)]^2}{N^2}}. \quad (8)$$

The average of  $\chi$  over 1000 noise realization was calculated for each input vector. Because of the chosen normalization,  $\chi$  can be seen as the average relative error of the retrieved elements of vector  $\tilde{J}$ . Fig. 4 shows the averaged  $\chi$  as a function of the relative phases differences 1-2 and 1-3 for  $\epsilon = 0.1$ . We notice that there is no preferential phase combination. The phase-averaged  $\chi$  grows linearly with the noise  $\epsilon$  with a slope of 0.7.

The fidelity of the modal analysis depends ultimately on how well the modes of the multimode waveguide describe the input field. A numerical estimate shows that a lateral shift of the input field by 1/32 of the waveguide diameter will change the projected amplitudes of the modes by  $\sim 10\%$ . We notice, however, that solid state lasers can feature a pointing stability better than 1/100 of the beam divergence.

To conclude, we proposed a fast and computationally inexpensive method for determining the complex amplitudes of the excited modes in a waveguide by means of intensity measurements. A single matrix multiplication is required to retrieve the sought-after coefficients, which implies that the method can be as fast as the photo-detection is. The method is, in principle, applicable to any number of modes; however, the array must have a number of waveguides that is at least equal to the square of the number of modes. The geometry of the lantern's SMFs, the geometry of the array, the manner by which the lantern is connected to the array, and the array's length all have an impact on how the modes evolve into the supermodes of the array. This, in

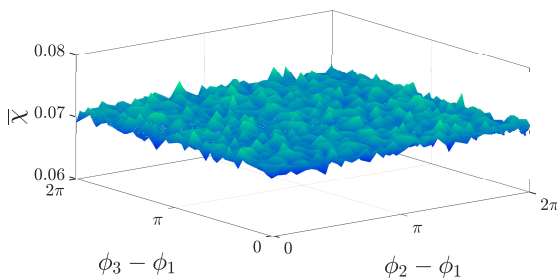


**Fig. 4.** The expected average relative error of the retrieved vector  $\tilde{J}$  from a noisy measurement of the output signal with the device depicted in Fig. 1. The horizontal axes represent the relative phase between modes 1-2 and 1-3. Only an additive Gaussian noise with standard deviation  $\epsilon = 0.1$  was considered in the calculation (see text for details).

turn, determines the condition number of the device's transfer matrix, which must be low to have a system that is relatively insensitive to measurement noise. The optimal configuration, shown by — in Fig. 2, has a low  $\kappa$  over a wide length range, which makes it suitable for broadband operation and makes it more tolerant to fabrication defects. A device like the one described here may be fabricated using 3D micro-fabrication techniques such as ultrafast laser inscription in glasses [21] or laser two-photon polymerization [22].

The device can be used to monitor the transverse modes in lasers for control purposes. The integrated mode analyzer could be matched directly to multimode fiber lasers or through free space optics to conventional laser cavities. The possibility to operate the device in real time opens its application in the control of the beam quality of fiber lasers [11] or of the oscillating mode in transverse multi-stable lasers [23].

**Funding.** German Federal Ministry of Education and Research (BMBF) (03Z22AN11).

## REFERENCES

1. J. Li, F. Ren, T. Hu, Z. Li, Y. He, Z. Chen, Q. Mo, and G. Li, *Opt. Fib. Techn.* **35**, 28 (2017).
2. T. Eidam, C. Wirth, C. Jauregui, F. Stutzki, F. Jansen, H.-J. Otto, O. Schmidt, T. Schreiber, J. Limpert, and A. Tünnermann, *Opt. Expr.* **19**, 13218 (2011).
3. J. W. Goodman, *Introduction to Fourier Optics* (W. H. Freeman, Englewood, Colo, 2004), 3rd ed.
4. T. Kaiser, D. Flamm, S. Schröter, and M. Duparré, *Opt. Expr.* **17**, 9347 (2009).
5. M. Paurisse, L. Lévêque, M. Hanna, F. Druon, and P. Georges, *Opt. Expr.* **20**, 4074 (2012).
6. J. W. Nicholson, A. D. Yablon, S. Ramachandran, and S. Ghalimi, *Opt. Expr.* **16**, 7233 (2008).
7. E. Narevicius, R. Narevich, Y. Berlatzky, I. Shtrichman, G. Rosenblum, and I. Vorobeichik, *Opt. Lett.* **30**, 3362 (2005).
8. N. Riesen, S. Gross, J. D. Love, and M. J. Withford, *Opt. Expr.* **22**, 29855 (2014).
9. N. Hanzawa, K. Saitoh, T. Sakamoto, T. Matsui, K. Tsujikawa, M. Koshihara, and F. Yamamoto, *Opt. Expr.* **22**, 29321 (2014).
10. S. G. Leon-Saval, N. K. Fontaine, J. R. Salazar-Gil, B. Ercan, R. Ryf, and J. Bland-Hawthorn, *Opt. Expr.* **22**, 1036 (2014).
11. H.-J. Otto, C. Jauregui, F. Stutzki, F. Jansen, J. Limpert, and A. Tünnermann, *Opt. Express* **21**, 17285 (2013).
12. S. Minardi and M. Diab, "Device for analyzing modes of multimode optical fibers," European patent application 18173928.5 - 1001 (May 23, 2018).
13. S. G. Leon-Saval, T. A. Birks, J. Bland-Hawthorn, and M. Englund, *Opt. Lett.* **30**, 2545 (2005).
14. S. Minardi and T. Pertsch, *Opt. Lett.* **35**, 3009 (2010).
15. A. Saviuk, S. Minardi, F. Dreisow, S. Nolte, and T. Pertsch, *Appl. Opt.* **52**, 4556 (2013).
16. W. H. Press, B. P. Flannery, S. A. Teukolsky, and W. T. Vetterling, *Numerical Recipes in C: The Art of Scientific Computing* (Cambridge University Press, Cambridge ; New York, 1992), 2nd ed.
17. S. Minardi, *Mon Not R Astron Soc* **422**, 2656 (2012).
18. S. Minardi, *Phys. Rev. A* **92**, 013804 (2015).
19. Synposys and RSoft Design Group, *RSoft, CAD & BeamPROP*, Synposys Inc, CA, USA (1993-2018).
20. T. A. Birks, I. Gris-Sánchez, S. Yerolatsitis, S. G. Leon-Saval, and R. R. Thomson, *Adv. Opt. Photon., AOP* **7**, 107 (2015).
21. R. R. Thomson, A. K. Kar, and J. Allington-Smith, *Opt. Express*, **OE** **17**, 1963 (2009).
22. R. Woods, S. Feldbacher, D. Zidar, G. Langer, V. Satzinger, V. Schmidt, N. Pucher, R. Liska, and W. Kern, *Opt. Mater. Express* **4**, 486 (2014).
23. C. Tamm and C. O. Weiss, *J. Opt. Soc. Am. B, JOSAB* **7**, 1034 (1990).



## FULL REFERENCES

1. J. Li, F. Ren, T. Hu, Z. Li, Y. He, Z. Chen, Q. Mo, and G. Li, "Recent progress in mode-division multiplexed passive optical networks with low modal crosstalk," *Opt. Fib. Techn.* **35**, 28–36 (2017).
2. T. Eidam, C. Wirth, C. Jauregui, F. Stutzki, F. Jansen, H.-J. Otto, O. Schmidt, T. Schreiber, J. Limpert, and A. Tünnermann, "Experimental observations of the threshold-like onset of mode instabilities in high power fiber amplifiers," *Opt. Expr.* **19**, 13218 (2011).
3. J. W. Goodman, *Introduction to Fourier Optics* (W. H. Freeman, Englewood, Colo, 2004), 3rd ed.
4. T. Kaiser, D. Flamm, S. Schröter, and M. Duparré, "Complete modal decomposition for optical fibers using CGH-based correlation filters," *Opt. Expr.* **17**, 9347 (2009).
5. M. Paurisse, L. Lévêque, M. Hanna, F. Druon, and P. Georges, "Complete measurement of fiber modal content by wavefront analysis," *Opt. Expr.* **20**, 4074 (2012).
6. J. W. Nicholson, A. D. Yablon, S. Ramachandran, and S. Ghalmi, "Spatially and spectrally resolved imaging of modal content in large-mode-area fibers," *Opt. Expr.* **16**, 7233 (2008).
7. E. Narevicius, R. Narevich, Y. Berlatzky, I. Shtrichman, G. Rosenblum, and I. Vorobeichik, "Adiabatic mode multiplexer for evanescent-coupling-insensitive optical switching," *Opt. Lett.* **30**, 3362–3364 (2005).
8. N. Riesen, S. Gross, J. D. Love, and M. J. Withford, "Femtosecond direct-written integrated mode couplers," *Opt. Expr.* **22**, 29855 (2014).
9. N. Hanzawa, K. Saitoh, T. Sakamoto, T. Matsui, K. Tsujikawa, M. Koshihara, and F. Yamamoto, "Mode multi/demultiplexing with parallel waveguide for mode division multiplexed transmission," *Opt. Expr.* **22**, 29321 (2014).
10. S. G. Leon-Saval, N. K. Fontaine, J. R. Salazar-Gil, B. Ercan, R. Ryf, and J. Bland-Hawthorn, "Mode-selective photonic lanterns for space-division multiplexing," *Opt. Expr.* **22**, 1036 (2014).
11. H.-J. Otto, C. Jauregui, F. Stutzki, F. Jansen, J. Limpert, and A. Tünnermann, "Controlling mode instabilities by dynamic mode excitation with an acousto-optic deflector," *Opt. Express* **21**, 17285 (2013).
12. S. Minardi and M. Diab, "Device for analyzing modes of multimode optical fibers," European patent application 18173928.5 - 1001 (May 23, 2018).
13. S. G. Leon-Saval, T. A. Birks, J. Bland-Hawthorn, and M. Englund, "Multimode fiber devices with single-mode performance," *Opt. Lett.* **30**, 2545 (2005).
14. S. Minardi and T. Pertsch, "Interferometric beam combination with discrete optics," *Opt. Lett.* **35**, 3009 (2010).
15. A. Saviuk, S. Minardi, F. Dreisow, S. Nolte, and T. Pertsch, "3d-integrated optics component for astronomical spectro-interferometry," *Appl. Opt.* **52**, 4556 (2013).
16. W. H. Press, B. P. Flannery, S. A. Teukolsky, and W. T. Vetterling, *Numerical Recipes in C: The Art of Scientific Computing* (Cambridge University Press, Cambridge ; New York, 1992), 2nd ed.
17. S. Minardi, "Photonic lattices for astronomical interferometry," *Mon Not R Astron Soc* **422**, 2656–2660 (2012).
18. S. Minardi, "Nonlocality of coupling and the retrieval of field correlations with arrays of waveguides," *Phys. Rev. A* **92**, 013804 (2015).
19. Synposys and RSoft Design Group, *RSoft, CAD & BeamPROP*, Synposys Inc, CA, USA (1993-2018).
20. T. A. Birks, I. Gris-Sánchez, S. Yerolatsitis, S. G. Leon-Saval, and R. R. Thomson, "The photonic lantern," *Adv. Opt. Photon., AOP* **7**, 107–167 (2015).
21. R. R. Thomson, A. K. Kar, and J. Allington-Smith, "Ultrafast laser inscription: an enabling technology for astrophotonics," *Opt. Express*, OE **17**, 1963–1969 (2009).
22. R. Woods, S. Feldbacher, D. Zidar, G. Langer, V. Satzinger, V. Schmidt, N. Pucher, R. Liska, and W. Kern, "3d optical waveguides produced by two photon photopolymerisation of a flexible silanol terminated polysiloxane containing acrylate functional groups," *Opt. Mater. Express* **4**, 486–498 (2014).
23. C. Tamm and C. O. Weiss, "Bistability and optical switching of spatial patterns in a laser," *J. Opt. Soc. Am. B, JOSAB* **7**, 1034–1038 (1990).